OPEN
10.1515/tvsb-2016-0017
Transactions of the VŠB – Technical University of Ostrava
Civil Engineering Series, No. 2, Vol. 16, 2016
paper #17

Juraj KRÁLIK[1] Juraj KRÁLIK, jr.[2] and Maroš KLABNÍK[3]

NONLINEAR ANALYSIS OF THE FAILURE OF NUCLEAR HERMETIC REINFORCED CONCRETE STRUCTURE DUE TO EXTREME PRESSURE AND TEMPERATURE

Abstract

This paper describes the nonlinear analysis of the reinforced concrete hermetic containment under an accidental temperature. The scenario of the hard accident in NPP and the methodology of the calculation of the failure temperature using the safety assessment are presented. The experimental and project material properties are taken into account in the safety assessment.

Keywords

Nuclear Power Plant, Containment, Nonlinearity, Failure temperature, ANSYS.

1 INTRODUCTION

After the accident of nuclear power plant (NPP) in Fukushimi the IAEA in Vienna adopted a large-scale project "Stress Tests of NPP", which defines new requirements for the verification of the safety and reliability of NPP under extreme effects of the internal and external environments and the technology accidents [9].

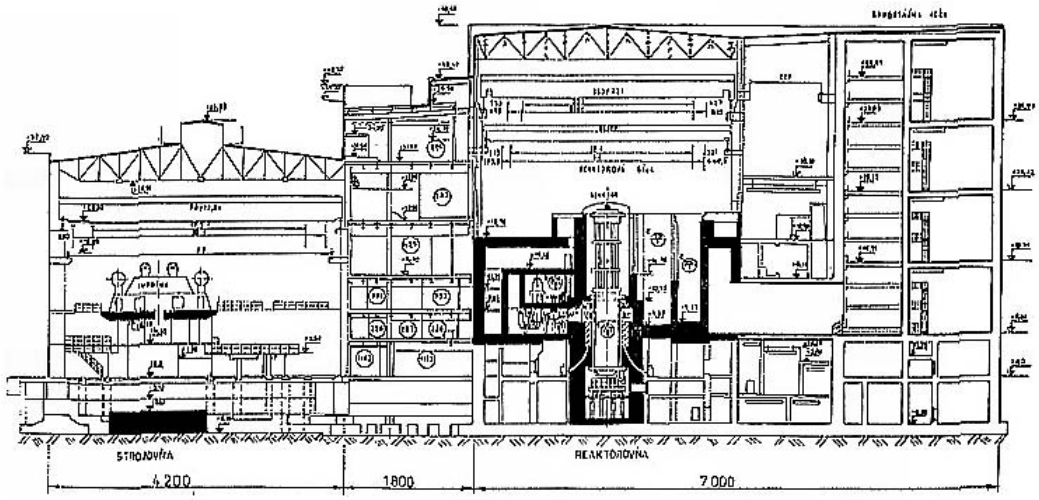

Fig. 1: Section plane of the NPP with reactor VVER440/213

[1] Prof. Ing. Juraj Králik, CSc, Department of Structural Mechanics, Faculty of Civil Engineering, STU Bratislava, Radlinského 11, 810 05 Bratislava, e-mail: juraj.kralik@stuba.sk.

[2] Ing. Juraj Králik, PhD, Institute of Constructions in Architecture and Engineering Structures, Faculty of Architecture, STU Bratislava, Námestie slobody 19, 812 45 Bratislava, kralik@fa.stuba.sk

[3] Ing. Maroš Klabník, Department of Structural Mechanics, Faculty of Civil Engineering, STU Bratislava, Radlinského 11, 810 05 Bratislava, maros.klabnik@stuba.sk

The experience from these activities will be used to develop a methodology in the frame of the project ALLEGRO, which is focused to the experimental research reactor of 4th generation with a fast neutron core. This project is a regional (V4 Group) project of European interest. The safety documents of NRC [19] and IAEA [11] initiate the requirements to verify the hermetic structures of NPP loaded by two combinations of the extreme actions. A first extreme load is considered for the probability of exceedance 10^{-4} by year and second for 10^{-2} by year. Other action effects are considered as the characteristic loads during the accident. In the case of the loss-of-coolant accident (LOCA) the steam pressure expand from the reactor hall to the bubble condenser [15]. The reactor and the bubble condenser reinforced structures with steel liner are the critical structures of the NPP hermetic zone [15, 15 and 17]. Next, one from the critical technology structures is the reactor hermetic cover.

2 SCENARIO OF THE ACCIDENT

The previous analysis was achieved for the overpressure value of 100kPa due to design basic accident (DBA), which corresponds of the loss of coolant accident due to guillotine cutting of the coolant pipe [15]. When the barbotage tower operates in the partial or zero performance the overpressure is equal to the 150 - 300 kPa. The ENEL propose the maximum temperature in the reactor shaft is equal about to 1.800°C and in the containment around the reactor shaft is equal about to 350°C [15]. The possibility of the temperature increasing to the containment failure state is considered in the scenario too. In the case of the hard accident the overpressure can be increased linearly and the internal and external temperature are constant. Three types of the scenarios were considered (Tab. 1).

Tab. 1: The assumed scenarios of the accidents in the hermetic zone

Type	Duration	Overpressure in HZ [kPa]	Extreme internal temperatures [°C]
I.	1hour - 1day	150	127
II.	2hours - 7days	250	150
III.	1year	-	80 - 120

The type III of accident scenario during 1 year with internal temperature 80-120°C and external temperature - 30°C was considered. The aim of this analysis was to determine the failure temperature.

3 CALCULATION MODEL

The NPP buildings with the reactor VVER 440/213 consists the turbine hall, middle building, reactor building and bubble condenser (Fig. 1). The main building of the NPP consists of the reactor objects, the steam generator box and the bubbler condenser. The finite element model (Fig. 2) is considered only the reinforced concrete structures of the steam generator box and the bubbler condenser. The steel structures are envisaged as the load on the reinforced concrete structures. The NPP model consists of a 4-node shell-elements (SHELL281) considering membrane, bending and shear stiffness, a solid elements (SOLID73) for the solution of the solid stress state of the massive reinforced concrete elements, a viscoelastic elements (COMBIN14) with the Winkler-Kelvin model of the soil, a point mass (MASS21) adequate to local load of the technology, a beam elements (BEAM4 and BEAM44) for columns and beams taking into account the membrane, bending and shear stiffness of beam members (LINK8) of the contact element (CE) and links (CP). The building of the power block was idealized with a FEM model consisting of 28 068 elements with 104 287 DOF (Fig. 2).

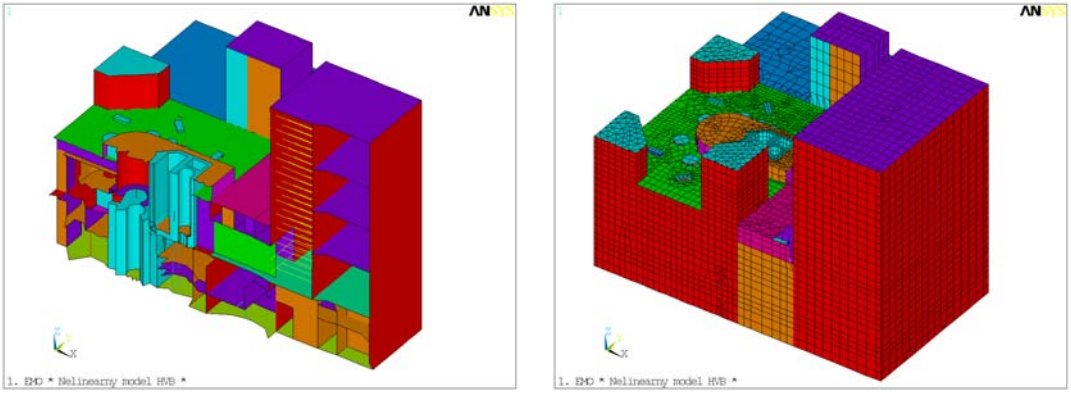

Fig. 2: Vertical section of the reactor with reactor protective hood

4 NON-LINEAR MODEL OF REINFORCED CONCRETE STRUCTURE

The theory of large strain and rate independent plasticity were proposed during the high overpressure loading using the SHELL181 layered shell element from (Fig. 3) the ANSYS library [13]. The vector of the displacement of the l^{th} shell layer

$$\{u^l\} = \{u_x^l, u_y^l, u_z^l\}^T$$

is approximated by the quadratic polynomial [15] in the form

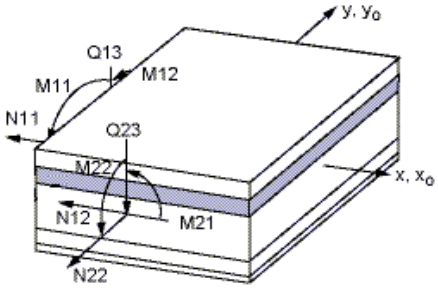

Fig. 3: SHELL181 layered element

$$\{u^l\} = \begin{Bmatrix} u_x^l \\ u_y^l \\ u_z^l \end{Bmatrix} = \sum_{i=1}^{4} N_i . \begin{Bmatrix} u_{xi} \\ u_{yi} \\ u_{zi} \end{Bmatrix} + \sum_{i=1}^{4} N_i . \frac{\zeta . t_i}{2} . \begin{bmatrix} a_{1,i} & b_{1,i} \\ a_{2,i} & b_{2,i} \\ a_{3,i} & b_{3,i} \end{bmatrix} . \begin{Bmatrix} \theta_{xi} \\ \theta_{yi} \end{Bmatrix} \tag{1}$$

where N_i is the shape function for i-node of the 4-node shell element, u_{xi}, u_{yi}, u_{zi} are the motion of i-node, ζ is the thickness coordinate, t_i is the thickness at i-node, $\{a\}$ is the unit vector in x direction, $\{b\}$ is the unit vector in plane of element and normal to $\{a\}$, θ_{xi} or θ_{yi} are the rotations of i-node about vector $\{a\}$ or $\{b\}$.

In the case of the elastic state the stress-strain relations for the l^{th} - layer are defined in the form

$$\{\sigma^l\} = [D_e^l]\{\varepsilon^l\} \tag{2}$$

where strain and stress vectors are as follows $\{\varepsilon^l\}^T = \{\varepsilon_x, \varepsilon_y, \gamma_{xy}, \gamma_{yz}, \gamma_{zx}\}$, $\{\sigma^l\}^T = \{\sigma_x, \sigma_y, \tau_{xy}, \tau_{yz}, \tau_{zx}\}$ and the matrix of the material stiffness

$$\left[D_e^l\right]=\begin{bmatrix} B^l E_x^l & B^l \mu_{xy}^l E_x^l & 0 & 0 & 0 \\ B^l \mu_{xy}^l E_x^l & B^l E_y^l & 0 & 0 & 0 \\ 0 & 0 & G_{xy}^l & 0 & 0 \\ 0 & 0 & 0 & \dfrac{G_{yz}^l}{k_s} & 0 \\ 0 & 0 & 0 & 0 & \dfrac{G_{zx}^l}{k_s} \end{bmatrix} \tag{3}$$

where $B^l = E_y^l \Big/ \left(E_y^l - \left(\mu_{xy}^l\right)^2 E_x^l\right)$, E_x^l (versus E_y^l) is Young modulus of the l^{th}-layer in the direction x (versus y), G_{xy}^l, G_{yz}^l, G_{zx}^l are shear moduli of the l^{th}-layer in planes XY, YZ and ZX; k_s is the coefficient of the effective shear area ($k_s = 1 + 0,2\,A/25t^2 \geq 1,2$), A is the element area, t is the element thickness.

4.1 Geometric nonlinearity

If the rotations are large but the mechanical strains (those that cause stresses) are small, then a large rotation procedure can be used. A large rotation analysis is performed in a static analysis in the ANSYS program [13].

The strain in the *n*-step of the solution can be computed from the relations

$$\{\varepsilon_n\} = [B_o][T_n]\{u_n\} \tag{4}$$

where $\{u_n\}$ is the deformation displacement, $[B_o]$ is the original strain-displacement relationship, $[T_n]$ is the orthogonal transformation relating the original element coordinates to the convected (or rotated) element coordinates. The convected element coordinate frame differs from the original element coordinate frame by the amount of rigid body rotation. Hence $[T_n]$ is computed by separating the rigid body rotation from the total deformation $\{u_n\}$ using the polar decomposition theorem.

4.1 Material nonlinearity

The presented constitutive model is a further extension of the smeared crack model [7], which was developed in [15]. Following the experimental results [3, 4, 6, 8, 12, 19, 20 and 21] a new concrete cracking layered finite shell element was developed and incorporated into the ANSYS system [15]. The layered approximation and the smeared crack model of the shell element are proposed.

The processes of the concrete cracking and crushing are developed during the increasing of the load. The concrete compressive stress fc, the concrete tensile stress ft and the shear modulus G are reduced after the crushing or cracking of the concrete [14].

In this model the stress-strain relation is defined (Fig. 4) following STN EN 1992-1-1

➲ Loading - compression region $\quad \varepsilon_{cu} < \varepsilon^{eq} < 0$

$$\sigma_c^{ef} = f_c^{ef} \cdot \frac{k.\eta - \eta^2}{1. + (k-2).\eta}, \qquad \eta = \frac{\varepsilon^{eq}}{\varepsilon_c} \quad , \quad (\varepsilon_c \doteq -0.0022\,,\ \varepsilon_{cu} \doteq -0.0035) \tag{5}$$

➲ Softening - compression region $\quad \varepsilon_{cm} < \varepsilon^{eq} < \varepsilon_{cu}$

$$\sigma_c^{ef} = f_c^{ef} \cdot \left(1 - \frac{\varepsilon^{eq} - \varepsilon_c}{\varepsilon_{cm} - \varepsilon_{cu}}\right) \tag{6}$$

➲ The tension region $\varepsilon_t < \varepsilon^{eq} < \varepsilon_m$

$$\sigma_c^{ef} = f_t.\exp(-2.(\varepsilon^{eq} - \varepsilon_t)/\varepsilon_{tm}), \qquad (\varepsilon_t \doteq 0.0001, \varepsilon_{tm} \doteq 0.002) \tag{7}$$

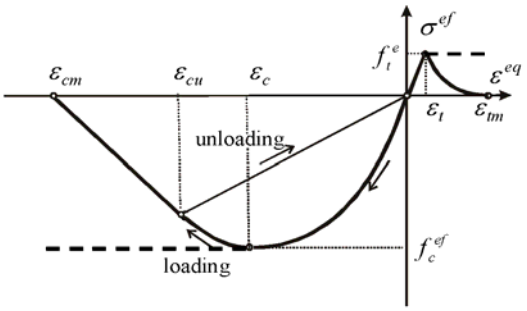

Fig. 4: The concrete stress-strain diagram

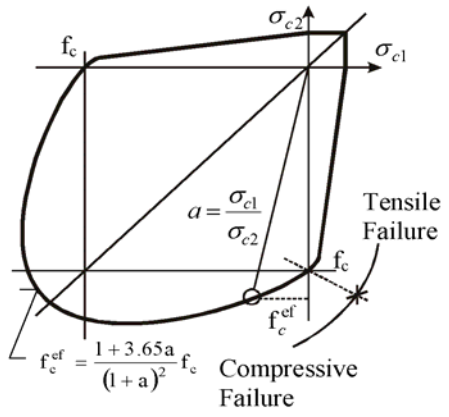

Fig. 5: Kupfer's plasticity function

In the case of the plane state the strength function in tension f_t and in compression f_c were considered equivalent values f_t^{eq} and f_c^{eq}.

In the plane of principal stresses (σ_{c1}, σ_{c2}) the relation between the one and bidimensional stresses state due to the plasticity function by Kupfer (see Fig. 5) can be defined as follows:

➲ Compression-compression

$$f_c^{ef} = \frac{1+3.65.a}{(1+a)^2}.f_c, \qquad a = \frac{\sigma_{c1}}{\sigma_{c2}} \tag{8}$$

➲ Tension-compression

$$f_c^{ef} = f_c.r_{ec}, \; r_{ec} = \left(1+5.3278\frac{\sigma_{c1}}{f_c}\right), \; r_{ec} \geq 0.9 \tag{9}$$

➲ Tension-tension

$$f_t^{ef} = f_t.r_{et}, \quad r_{et} = \frac{A+(A-1).B}{A.B}, \quad B = K.x + A,$$
$$x = \sigma_{c2}/f_c, \quad r_{et} = 1. \Leftrightarrow x = 0 \qquad r_{et} = 0.2 \Leftrightarrow x = 1 \tag{10}$$

The shear concrete modulus G was defined for cracking concrete by Kolmar [14] in the form

$$G = r_g.G_o, \; r_g = \frac{1}{c_2}\ln\left(\frac{\varepsilon_u}{c_1}\right), \; c_1 = 7+333(p-0{,}005), \; c_2 = 10-167(p-0.005) \tag{11}$$

where G_o is the initial shear modulus of concrete, ε_u is the strain in the normal direction to crack, c_1 and c_2 are the constants dependent on the ratio of reinforcing, p is the ratio of reinforcing transformed to the plane of the crack ($0 < p < 0.02$).

It is proposed that the crack in the one layer of shell element is oriented perpendicular to the orientation of principal stresses. The membrane stress and strain vector depends on the direction of the principal stress and strain in one layer

$$\{\varepsilon_{cr}\} = [T_\varepsilon]\{\varepsilon\}, \qquad \{\sigma_{cr}\} = [T_\sigma]\{\sigma\} \tag{12}$$

where $[T_\varepsilon]$, $[T_\sigma]$ are transformation matrices for the principal strain and stress in the direction θ in the layer.

The strain-stress relationship in the Cartesian coordinates can be defined in dependency on the direction of the crack (in the direction of principal stress, versus strain)

$$[\sigma_{cr}] = [D_{cr}]\{\varepsilon_{cr}\} \text{ and } [\sigma] = [T_\sigma]^{\mathrm{T}}[D_{cr}][T_\varepsilon]\{\varepsilon\} \tag{13}$$

For the membrane and bending deformation of the reinforced concrete shell structure the layered shell element, on which a plane state of stress is proposed on every single layer, was used.

The stiffness matrix of the reinforced concrete for the l^{th}-layer can be written in the following form

$$\left[D_{cr}^{l}\right] = \left[T_{c.\sigma}^{l}\right]^{\mathrm{T}}\left[D_{cr}^{l}\right]\left[T_{c.\varepsilon}^{l}\right] + \sum_{s=1}^{N_{rein}}\left[T_s^{l}\right]^{\mathrm{T}}\left[D_s^{l}\right]\left[T_s^{l}\right] \tag{14}$$

where $[T_{c.\sigma}]$, $[T_{c.\varepsilon}]$, $[T_s]$ are the transformation matrices for the concrete and the reinforcement separately, N_{rein} is the number of the reinforcements in the l^{th} - layer.

After cracking the elasticity modulus and Poisson's ratio are reduced to zero in the direction perpendicular to the cracked plane, and a reduced shear modulus is employed. Considering 1 and 2 two principal directions in the plane of the structure, the stress-strain relationship for the concrete l^{th} - layer cracked in the 1-direction, is

$$\begin{Bmatrix}\sigma_1\\ \sigma_2\\ \tau_{12}\\ \tau_{13}\\ \tau_{23}\end{Bmatrix}_l = \begin{bmatrix}0 & 0 & 0 & 0 & 0\\ 0 & E & 0 & 0 & 0\\ 0 & 0 & G_{12}^{cr} & 0 & 0\\ 0 & 0 & 0 & G_{13}^{cr} & 0\\ 0 & 0 & 0 & 0 & G_{23}^{cr}\end{bmatrix}_l \begin{Bmatrix}\varepsilon_1\\ \varepsilon_2\\ \gamma_{12}\\ \gamma_{13}\\ \gamma_{23}\end{Bmatrix}_l \tag{15}$$

where the shear modulus are reduced by the coefficient of the effective shear area k_s and parameter r_{g1} by Kolmar (11) as follows:

$$G_{12}^{cr} = G_o.r_{g1}, \quad G_{13}^{cr} = G_o.r_{g1}, \quad G_{23}^{cr} = G_o / k_s$$

When the tensile stress in the 2-direction reaches the value f_t', the latter cracked plane perpendicular to the first one is assumed to form, and the stress-strain relationship becomes:

$$\begin{Bmatrix}\sigma_1\\ \sigma_2\\ \tau_{12}\\ \tau_{13}\\ \tau_{23}\end{Bmatrix}_l = \begin{bmatrix}0 & 0 & 0 & 0 & 0\\ 0 & 0 & 0 & 0 & 0\\ 0 & 0 & G_{12}^{cr}/2 & 0 & 0\\ 0 & 0 & 0 & G_{13}^{cr} & 0\\ 0 & 0 & 0 & 0 & G_{23}^{cr}\end{bmatrix}_l \begin{Bmatrix}\varepsilon_1\\ \varepsilon_2\\ \gamma_{12}\\ \gamma_{13}\\ \gamma_{23}\end{Bmatrix}_l \tag{16}$$

where the shear moduli are reduced by the parameter r_{g1} and r_{g2} by Kolmar (11) as follows:

$$G_{12}^{cr} = G_o.r_{g1}, \quad G_{13}^{cr} = G_o.r_{g1}, \quad G_{23}^{cr} = G_o r_{g2}.$$

The cracked concrete is anisotropic and these relations must be transformed to the reference axes *XY*. The simplified averaging process is more convenient for finite element formulation than the singular discrete model. A smeared representation for the cracked concrete implies that cracks are not discrete but distributed across the region of the finite element. The cracked concrete is anisotropic and these relations must be transformed to the reference axes *XY*. The simplified averaging process is more convenient for finite element formulation than the singular discrete model. A smeared representation for the cracked concrete implies that cracks are not discrete but distributed across the region of the finite element.

The smeared crack model [3, 7], used in this work, results from the assumption, that the field of more micro cracks (not one local failure) brought to the concrete element will be created. The validity of this assumption is determined by the size of the finite element, hence its characteristic dimension $L_c = \sqrt{A}$, where A is the element area (versus integrated point area of the element). For the expansion of cracking the assumption of constant failure energies G_f=*const* is proposed in the form

$$G_f = \int_0^\infty \sigma_n(w)\,dw = A_G.L_c\,, \qquad w_c = \varepsilon_w.L_c \tag{17}$$

where w_c is the width of the failure, σ_n is the stress in the concrete in the normal direction, A_G is the area under the stress-strain diagram of concrete in tension. Concrete modulus for descend line of stress strain diagram in tension (crushing) can be described according to Oliver [7] in dependency on the failure energies in the form

$$E_{c,s} = E_c/(1-\lambda_c)\,, \qquad \lambda_c = 2G_f E_c/\left(L_c.\sigma_{\max}^2\right) \tag{18}$$

where E_c is the initial concrete modulus elasticity, σ_{max} is the maximal stress in the concrete tension. From the condition of the real solution of the relation (18) it follows, that the characteristic dimension of element must satisfy the following condition

$$L_c \le 2G_f E_c/\sigma_{\max}^2 \tag{19}$$

The characteristic dimension of the element is determined by the size of the failure energy of the element. The theory of a concrete failure was implied and applied to the 2D layered shell elements SHELL181 in the ANSYS element library [13]. The CEB-FIP Model Code [5] define the failure energies G_f [N/mm] depending on the concrete grades and the aggregate size d_a as follows

$$G_f = \left(0.0469d_a^2 - 0.5d_a + 26\right)\left(f_c/10\right)^{0.7} \tag{20}$$

The limit of damage at a point is controlled by the values of the so-called crushing or total failure function F_u. The modified Kupfer's condition for the l^{th}-layer of section is following

$$F_u^l = F_u^l\left(I_{\varepsilon 1}; I_{\varepsilon 2}; \varepsilon_u\right) = 0\,, \quad F_u^l = \sqrt{\beta\left(3J_{\varepsilon 2} + \alpha I_{\varepsilon 1}\right)} - \varepsilon_u = 0\,, \tag{21}$$

where $I_{\varepsilon l}$, $J_{\varepsilon 2}$ are the strain invariants, and ε_u is the ultimate total strain extrapolated from uniaxial test results ($\varepsilon_u = 0.002$ in the tension domain, or $\varepsilon_u = 0.0035$ in the compression domain), α, β are the material parameters determined from the Kupfer's experiment results ($\beta = 1.355,\ \alpha = 0.355\varepsilon_u$).

The failure function of the whole section will be obtained by the integration of the failure function through to the whole section in the form

$$F_u = \frac{1}{t}.\int_0^t F_u^l\left(I_{\varepsilon 1}; I_{\varepsilon 2}; \varepsilon_u\right)dz = \frac{1}{t}\sum_{l=1}^{N_{lay}} F_u^l\left(I_{\varepsilon 1}; I_{\varepsilon 2}; \varepsilon_u\right)t_l \tag{22}$$

where t_l is the thickness of the l^{th} - shell layer, t is the total shell thickness and N_{lay} is the number of layers.

The collapse state of the reinforced concrete structure is determined by the maximum strain ε_s of the reinforcement steel in the tension area ($\max\left(\varepsilon_s\right) \le \varepsilon_{sm} = 0.01$) and by the maximum concrete crack width w_c ($\max\left(w_c\right) \le w_{cm} = 0.3\,\text{mm}$).

The program CRACK based on the presented nonlinear theory of the layered reinforced concrete shell was adopted in the software ANSYS [15, 17]. These procedures were tested in comparison with the experimental results [15].

5 REINFORCED CONCRETE STRUCTURES UNDER HIGH TEMPERATURE IMPACT

The mechanical properties of the concrete under high temperature impact were considered in the research laboratory in Slovakia and Czech [2, 4 and 12] and abroad [8 and 20]. The recapitulation of the research works and the standard recommendations of the concrete under high temperature effect are summarized in US NRC report [19]. The recommendations for the design of the reinforced concrete structures are described in the US standards ACI [1] as well as the CEB-FIP Model Code [5] and Eurocodes [10].

On the base of the research results in domain of the concrete and steel behaviour of the reinforced concrete structures under the temperature effect the US standards [1 and 19], EU standards [10] and IAEA recommendations [11] determine the basic material characteristics for the numerical analysis and design of the RC structural element.

The bonding phases of concrete are from the instable substance, which can be destructed at high temperature and their microstructures are changed. The processes in the cement bond and the concrete due to high temperature were investigated by many authors [2, 8 and 20].

The thermal conductivity λ_c of normal weight concrete may be determined between the lower and upper limits given hereafter. The upper limit has been derivated from tests of steel-concrete composite structural elements. The use of the upper limit is recommended in Eurocode EN1992-1-2 [10].

The upper limit of thermal conductivity λ_c of normal weight concrete may be determined from:

$$for\ 20^oC \le \theta_c \le 1200^oC: \quad \lambda_c = 2 - 0.2451(\theta_c/100) + 0.0107(\theta_c/100)^2\ [W/mK]\ , \qquad (23)$$

where θ_c is the concrete temperature.

The lower limit of thermal conductivity λ_c of normal weight concrete may be determined from:

$$for\ 20^oC \le \theta_c \le 1200^oC: \quad \lambda_c = 1.36 - 0.136(\theta_c/100) + 0.0057(\theta_c/100)^2\ [W/mK] \qquad (24)$$

In simple calculation models the thermal conductivity may be considered to be independent of the concrete temperature. In this case the following value [10] should be taken:

$$\lambda_c = 1.30\ [W/mK] \qquad (25)$$

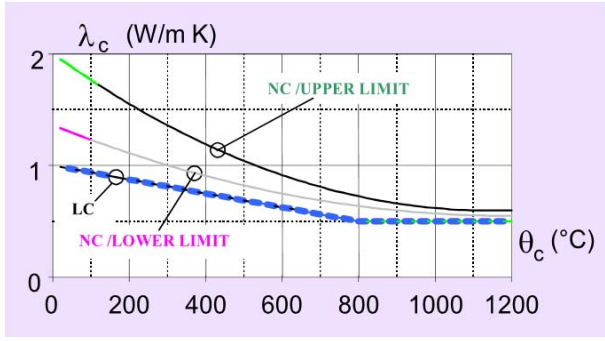

Fig. 6: Thermal conductivity of concrete as a function of temperature [10]

The thermal conductivity λ_a of steel valid for all structural and reinforcing steel qualities may be determined from following:

$$for\ 20^oC \le \theta_a \le 800^oC: \quad \lambda_a = 54 - 3.33(\theta_a/100)\ [W/mK] \qquad (26)$$

$$for\ 800^oC \le \theta_a \le 1200^oC: \quad \lambda_a = 27.3\ [W/mK]$$

where θ_a is the steel temperature.

In simple calculation models the thermal conductivity may be considered to be independent of the steel temperature. In this case the following value [10] should be taken:

$$\lambda_c = 45\,[W/mK] \tag{27}$$

The Eurocode EN1992-1-2 [10] define the stress-strain relationship for concrete and steel materials dependent on temperature for heating rates between 2 and 50K/min. In the case of the concrete the stress-strain diagram is divided on two regions. The concrete strength increase in first region and decrease in second region (Fig.7).

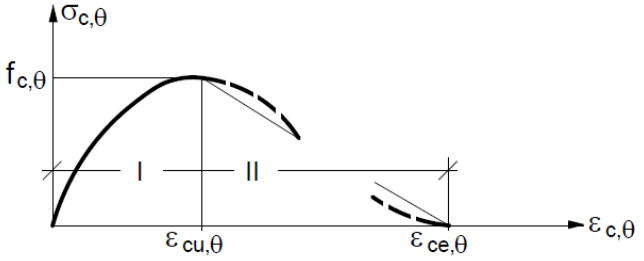

Fig. 7: Stress-strain relationship of the concrete dependent on temperature [10]

The stress-strain relation $\sigma_{c,\theta} \approx \varepsilon_{c,\theta}$ in region I are defined in following form:

$$\sigma_{c,\theta} = f_{c,\theta}\left[3\left(\frac{\varepsilon_{c,\theta}}{\varepsilon_{cu,\theta}}\right)\Big/\left\{2+\left(\frac{\varepsilon_{c,\theta}}{\varepsilon_{cu,\theta}}\right)^3\right\}\right], \qquad f_{c,\theta} = k_{c,\theta} f_c\ , \tag{28}$$

where the strain $\varepsilon_{cu,\theta}$ corresponds to stress $f_{c,\theta}$, the reduction factor can be chosen according to standard [10]. The reduction factors $k_{c,\theta}$ $\left(k_{c,\theta} = 0.25\ for\ \theta_c = 150^o C\right)$ for the stress-strain relationship are considered in accordance with the standard.

The stress-strain relationship for the steel (Fig.8) are considered in accordance of Eurocode [10] on dependency of temperature level θ for heating rates between 2 and 50K/min in the case of the steel the stress-strain diagram is divided on four regions.

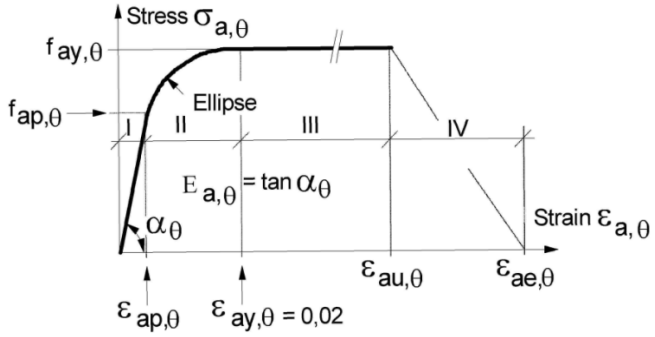

Fig. 8: Stress-strain relationship of the steel dependent on temperature [10]

The stress-strain relations $\sigma_{a,\theta} \approx \varepsilon_{a,\theta}$ are defined in following form in region I:

$$\sigma_{a,\theta} = E_{a,\theta}\varepsilon_{a,\theta}\ , \qquad E_{a,\theta} = k_{E,\theta} E_a \tag{29}$$

where the reduction factor $k_{E,\theta}$ can be chosen according to the standard [10].

In region II :

$$\sigma_{a,\theta} = \left(f_{ay} - c\right) + \frac{b}{a}\sqrt{a^2 - \left(\varepsilon_{ay,\theta} - \varepsilon_{a,\theta}\right)^2}\,, \quad a^2 = \left(\varepsilon_{ay,\theta} - \varepsilon_{ap,\theta}\right)\left(\varepsilon_{ay,\theta} - \varepsilon_{ap,\theta} + c/E_{a,\theta}\right), \qquad (30)$$

$$b^2 = E_{a,\theta}\left(\varepsilon_{ay,\theta} - \varepsilon_{ap,\theta}\right)c + c^2\,, \qquad c = \frac{\left(f_{ay,\theta} - f_{ap,\theta}\right)^2}{E_{a,\theta}\left(\varepsilon_{ay,\theta} - \varepsilon_{ap,\theta}\right) - 2\left(f_{ay,\theta} - f_{ap,\theta}\right)}$$

and in region III :

$$\sigma_{a,\theta} = f_{ay,\theta} \qquad (31)$$

A graphical display of the stress-strain relationships for steel grade S235 is presented in Fig. 8 up to a maximum strain $\varepsilon_{ay,\theta} = 2\%$.

The strength and deformation properties of reinforcing steels as elevated temperatures may be obtained by the same mathematical model as that presented for structural steel S235. The reduction factors $k_{E,\theta}$ $\left(k_{E,\theta} = 0.95\ for\ \theta_a = 150^o C\right)$ for the stress-strain relationship are considered in accordance with the standard [10].

6 NONLINEAR DETERMINISTIC ANALYSIS

The critical sections of the structure were determined on the base of the nonlinear analysis due to the monotone increasing of temperature inside the hermetic zone [15, 17]. The resistance of these critical sections was considered taking into account the design values of the material characteristics and the load. The combination load and design criteria were considered for the extreme state as the hard accident in accordance with the international standard [11].

The critical areas were identified on base of nonlinear analysis in the plate at level +18.9m in SG box, next at level +6.0m in the corridor between SG box and the bubbler tower. The results from the linear and nonlinear analysis are compared in fig. 9 and 10.

The interior structures of the hermetic zone are loaded with the accident temperature equal to 150ºC and the outside structures in the contact with the exterior are loaded by -30ºC. The difference between the interior end the exterior temperature has the significant influences to the peak strain in the structures.

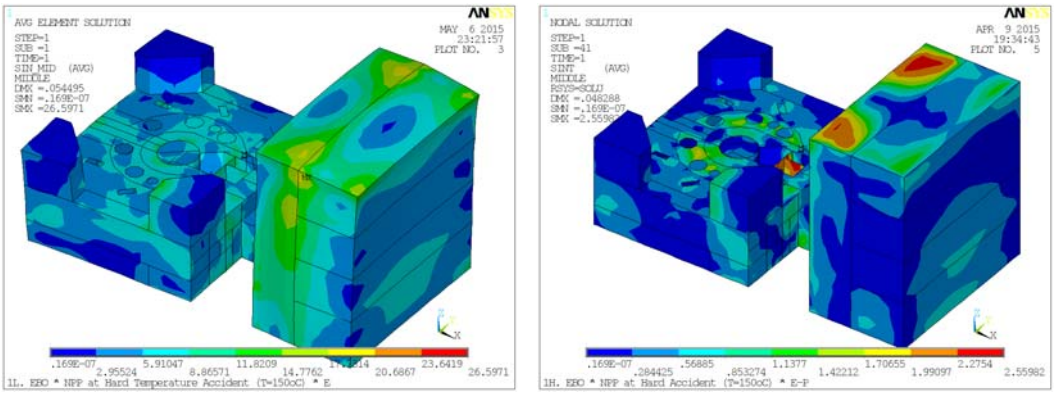

Fig. 9: Stress intensity from the linear and nonlinear analysis

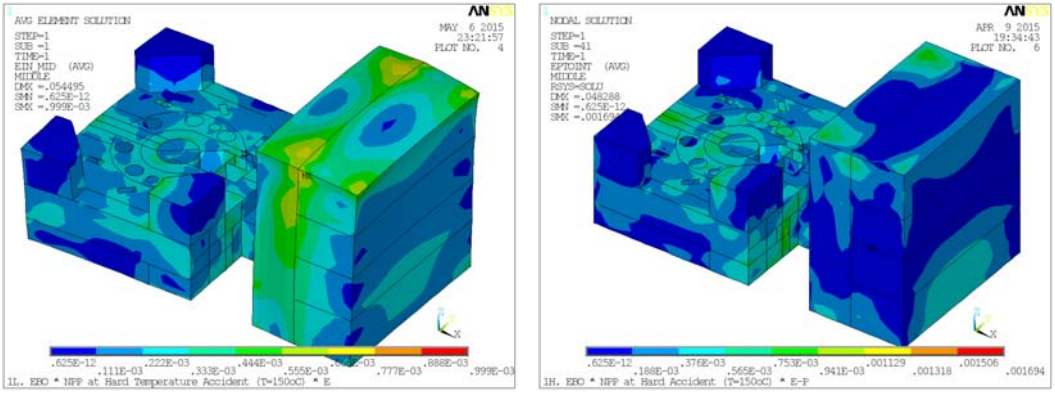

Fig. 10: Strain intensity from the linear and nonlinear analysis

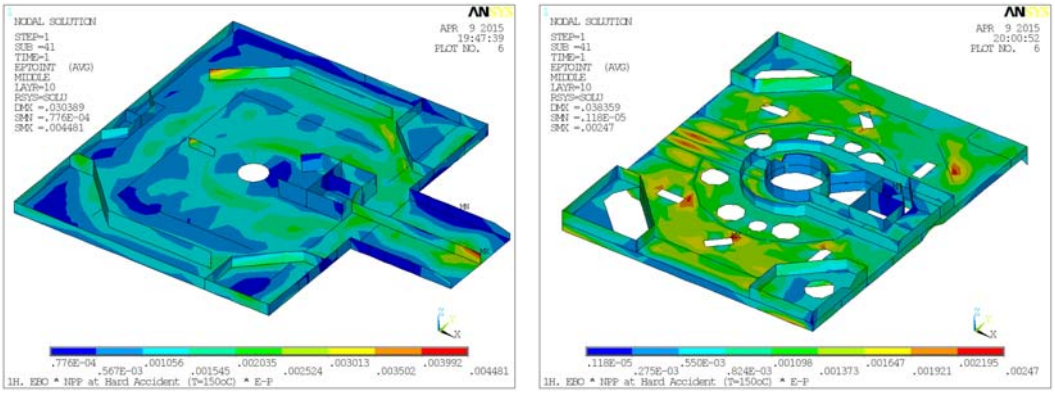

Fig. 11: Maximum strain intensity in top shell layer at level +6.0m and +18.9m

Tab. 2: Recapitulation of the critical areas in the hermetic RC structures

Node	Layer	Maximum principal strain at bottom/middle/top layered shell				
		ε_1	ε_2	ε_3	ε_{int}	ε_{eqv}
Room V3 at level +18,9m in module G/17						
3907	1	2.08E-03	-6.12E-04	-1.56E-03	3.64E-03	2.20E-03
3907	5	6.67E-04	-1.08E-04	-6.51E-04	1.32E-03	7.86E-04
3907	10	9.86E-04	5.54E-04	-1.44E-03	2.43E-03	1.52E-03
Corridor plate at level +6m in module G-D/13-15						
1392	1	4.46E-04	3.57E-04	-8.48E-04	1.29E-03	9.14E-04
1392	5	6.52E-04	9.69E-05	-8.23E-04	1.48E-03	9.26E-04
1392	10	1.22E-03	-4.09E-04	-9.04E-04	2.12E-03	1.32E-03
Corridor plate at level +6m in module G-D/13-15						
2086	1	7.53E-04	-2.16E-04	-4.62E-04	1.22E-03	8.14E-04
2086	5	3.32E-04	3.22E-04	-6.99E-04	1.03E-03	7.69E-04
2086	10	1.82E-03	-4.04E-04	-1.51E-03	3.34E-03	2.01E-03

The comparison of the stress shape from the linear and nonlinear solution is compared in Fig. 9 and the strain shape in Fig. 10 and 11. The strain increase and the stress decrease in the nonlinear solution in comparison with the linear solution.

The intensity of the stress values are about 10x lower and the intensity of the strain values are about 17x higher and in the nonlinear analysis in comparison with the linear analysis. These facts are in consequence with the consideration of the cracking process in the reinforced concrete structures during the extreme loads.

7 SAFETY AND RELIABILITY ANALYSIS OF THE HERMETIC STRUCTURES

In the case of the severe accidents defined beyond the initial design criteria of NPP structures, the safety and reliability of the containment integrity assessed beyond the standard design criteria defined in design standards for new structures. The main criterion is the requirement to stopped the leaking radioactivity into the environment and to ensure the tightness of containment. The concrete cracking process arrive due to high temperature gradient between interior (150°C) and exterior (-30°C) temperature. In the concrete walls (resp. plates) the shear cracks occur due to the difference temperature in the mid-plane along the contact of two surfaces with different temperatures of occurrence of tensile stresses, involving the concrete will crack. The concrete slabs the cracks due to the bending temperature gradient between the inner and the outer plate surface. In the case of board-wall structures for combined membrane and bending stress state. The bending cracks arrive due to temperature gradient between bottom and top surface of concrete plate. In the case of the walls the combination of the membrane and bending stress state is deciding. In the case of the nonlinear analysis the failure mode of the reinforced concrete structure is determined by the failure function depended on the principal deformations in the reinforcement in tension area of section.

8 CONCLUSIONS

The nonlinear analysis of the containment failure is in accordance with the requirements IAEA [11] and NRC [19], experiences from the similar analysis NPP in abroad [19, 20], new knowledges from the analysis of structures [15] and our experiences from the previous analysis [15, 16 and 17]. The nonlinear analysis of the loss of the concrete containment integrity was made for the accident temperature 150°C and the extreme climatic temperature -30°C using the nonlinear solution of the static equilibrium considering the geometric and material nonlinearities of the reinforced concrete shell layered elements. The nonlinear analyses were performed in the CRACK program, which was developed by the author and implemented into the ANSYS system [15]. The reliability function RF was defined in dependency on the failure function $F_u(I_{\varepsilon 1}; J_{\varepsilon 2}; \varepsilon_u)$ for requirements of the IAEA.

According to the nonlinear deterministic analysis were defined the most critical structural components for which the values of the failure pressure of the accident are determined on base of the best estimation. We propose from the supposition that the loss of containment integrity occur and the performance of the NPP can be unsafe.

The maximum principal strain in the reinforcement layer is equal to $\max.\varepsilon_1 = 0.00208$ $\left(\varepsilon_{ay,\theta} < \varepsilon_1 < \varepsilon_{au,\theta}\right)$. The maximum principal strain is higher than the yield strain, but lower as unlimited strain. The estimated failure temperature is equal to $T_u = 570^o C$, for which the reduction factor of concrete is $k_{c,\theta} = 0.676$ and steel reinforcement $k_{u,\theta} = 0.563$ [10].

ACKNOWLEDGMENT

The project was performed with the financial support of the Grant Agency of the Slovak Republic (VEGA 1/0265/16).

LITERATURE

[1] ACI 349-90, "*Code Requirements for Nuclear Safety Related Concrete Structures*", American Concrete Institute, Detroit, 1990 and 1996.

[2] BAYER, P. MATESOVÁ, D. Vliv endotermických reakcí rozkladu fází cementového tmelu v betonu na jeho pórovou strukturu. In proc. : *PPK 2006. Rep. of papers from II. International conference*, 3. - 4. 10. 2006, FAST VUT Brno, pp. 19 - 26. ISBN 80-214-3251-9.

[3] BAŽANT, Z. P. PANG, S. D. VOŘECHOVSKÝ, M. and NOVÁK. D. Energetic-statistical size effect simulated by SFEM with stratified sampling and crack band model. *International Journal for Numerical Methods in Engineering* (Wiley), 71(11):1297-1320, 2007, Rep. Department of Civil Engineering, Northwestern University, Evanston, Illinois.

[4] BROŽOVSKÝ, J. KONEČNÝ, P. MYNARZ M. SUCHARDA, O. Comparison of Alternatives for Remodelling of Laboratory Tests of Concrete, In *Proceedings of the Twelfth International Conference on Civil, Structural and Environmental Engineering Computing*, B.H.V. Topping, L.F. Costa Neves, R.C. Barros, (Editors), Funchal: Civil-Comp Press (Stirlingshire), paper 119, 2009. ISBN 978-1-905088-30-0.

[5] CEB-FIP Model Code. *Design Code*, Thomas Telford, 1990, ISBN 0727716964.

[6] ČAJKA, R. KREJSA, M. Measured Data Processing in Civil Structure Using the DOProC, Method, *Advanced Materials Research* Vol. 859, p. 114-121, DOI 10.4028/www.scientific.net / AMR.859.114, December, 2013 .

[7] ČERVENKA, V. Constitutive Model for Cracked Reinforced Concrete, *ACI Journal* 82, 877, 1985.

[8] CHAN, S. Y. N. WEI SUNB, X. L. Effect of high temperature and cooling regimes on the compressive strength and pore properties of high performance concrete. *Construction and Building Materials* 14, 261-266.

[9] ENSREG, Post-Fukushima accident. Action Plan. Follow-up of the peer review of the stress tests performed on European nuclear power plants, 2012.

[10] EUROCODE 2: Design of concrete structures - Part 1-2: General rules - Structural fire design. The European Union Per Regulation 305/2011, Directive 98/34/EC, Directive 2004/18/EC.

[11] IAEA, Safety Series No. NS-G-1.10, Design of Reactor Containment Systems for Nuclear Power Plants, IAEA Vienna, 2001.

[12] JERGA, J. and KRIŽMA, M. Assessment of Concrete Damage, *Building Research Journal* 54, 2006, p.211.

[13] KOHNKE, P., 2008. *ANSYS, Theory*, SAS IP Inc. Canonsburg.

[14] KOLMAR, W. Beschreibung der Kraftübertragung über Risse in nichtlinearen Finite-Element-Berechnungen von Stahlbeton-tragwerken, PhD Thesis, T.H. Darmstadt, Darmstadt, 1986.

[15] KRÁLIK, J. Safety and Reliability of Nuclear Power Buildings in Slovakia. Earthquake-Impact-Explosion. Ed. STU Bratislava, 2009, 307pp. ISBN 978-80-227-3112-6.

[16] KRÁLIK, J. Reliability Analysis of Structures Using Stochastic Finite Element Method, Ed. STU Bratislava, 2009, 143pp. ISBN 978-80-227-3130-0.

[17] KRÁLIK, J. et al. Structural Reliability for Containment of VVER 440/213 Type, In *Safety and Reliability: Methodology and Applications - Nowakowski et al.* (Eds) © 2015 Taylor & Francis Group, London, p.2279-2286.

[18] NOVÁK, D. BERGMEISTER, K. PUKL, R. ČERVENKA, V. Structural assessment and reliability analysis for existing engineering structures, Theoretical background. *Structure and infrastructure engineering*, Vol. 9, No. 2, 2009, pp. 267-275.

[19] NUREG/CR-7031, A Compilation of Elevated Temperature Concrete Material Property Data and Information for Use in Assessments of Nuclear Power Plant Reinforced Concrete Structures, ORNL/TM-2009/175, US NRC, 2010.

[20] SCHNEIDER, U. & SCHWESINGER, P. Mechanical Testing of Concrete at High Temperature, *RILEM-U*, Kassel - U. Weimar, Kassel, 1990, p. 20-21.

[21] SUCHARDA, O., BROŽOVSKÝ, J., MIKOLÁŠEK, D. Numerical Modelling and Bearing Capacity of Reinforced Concrete Beams. *Key Engineering Materials*, 2014, pp. 281-284.